Volume 20 | Number 6 | 14 February 2018 | Pages 3853–4608

PCCP

Physical Chemistry Chemical Physics

rsc.li/pccp

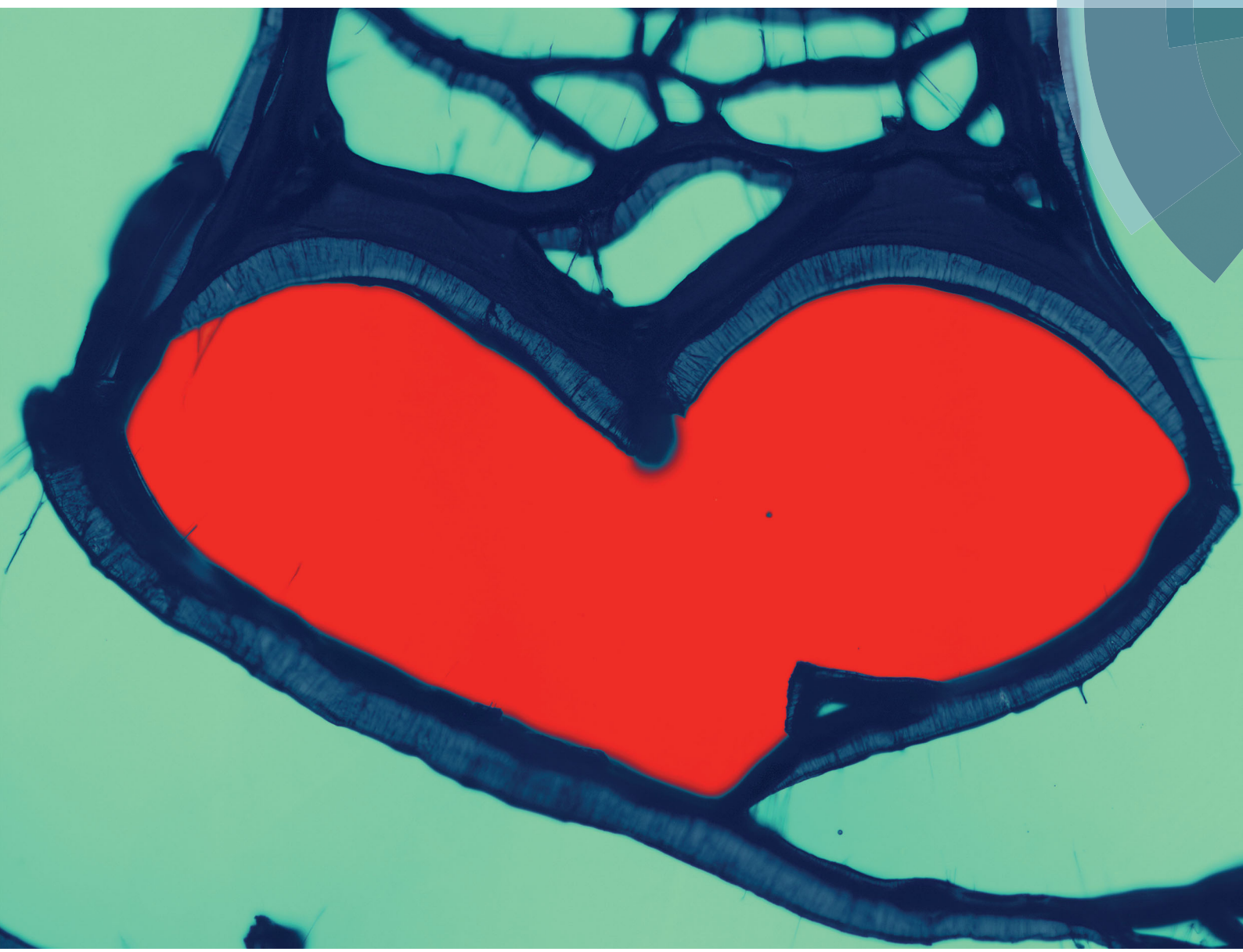

ISSN 1463-9076

ROYAL SOCIETY OF CHEMISTRY

COMMUNICATION

Itai Y. Stein, Brian L. Wardle *et al.*

Process-morphology scaling relations quantify self-organization in capillary densified nanofiber arrays

PCCP

COMMUNICATION

View Article Online
View Journal | View Issue

Cite this: *Phys. Chem. Chem. Phys.*, 2018, **20**, 3876

Received 9th October 2017,
Accepted 2nd January 2018

DOI: 10.1039/c7cp06869g

rsc.li/pccp

Process-morphology scaling relations quantify self-organization in capillary densified nanofiber arrays†

Ashley L. Kaiser, ‡[a] Itai Y. Stein, ‡*[b] Kehang Cui [c] and Brian L. Wardle *[b]

Capillary-mediated densification is an inexpensive and versatile approach to tune the application-specific properties and packing morphology of bulk nanofiber (NF) arrays, such as aligned carbon nanotubes. While NF length governs elasto-capillary self-assembly, the geometry of cellular patterns formed by capillary densified NFs cannot be precisely predicted by existing theories. This originates from the recently quantified orders of magnitude lower than expected NF array effective axial elastic modulus (*E*), and here we show *via* parametric experimentation and modeling that *E* determines the width, area, and wall thickness of the resulting cellular pattern. Both experiments and models show that further tuning of the cellular pattern is possible by altering the NF–substrate adhesion strength, which could enable the broad use of this facile approach to predictably pattern NF arrays for high value applications.

The potential for meter-scale bulk manufacturing and unique anisotropic physical properties of one-dimensional nanostructures, such as nanowires, nanotubes, and nanofibers (NFs), motivates their use in industrial applications, such as electrical interconnects,[1–4] energy harvesting and storage,[4–8] sensors and actuators,[9–12] and structural reinforcement.[13–15] However, the low packing density and inherent stochastic nature of these NFs when synthesized by scalable approaches, such as chemical vapor deposition, leads to observed properties that are orders of magnitude lower than expected.[16–18] This could be substantially overcome by densification approaches such as capillary-mediated densification, which is a versatile and scalable approach that has been utilized to increase the packing density and form intricate three-dimensional nano-architectures out of aligned NF systems.[19–22] But since NFs self-organize into two-dimensional cellular structures of unpredictable shapes and sizes when this approach is applied to bulk NF arrays $\gtrsim$100 μm tall,[20–22] models that predict cellular network formation are needed. Here, we develop process-morphology scaling relations that quantify and accurately predict the self-organization of an exemplary system of NFs, aligned carbon nanotube (CNT) arrays, into cellular patterns, and show that the effective elastic modulus scaling of the cell wall with its height governs the wall thickness, width, and area of the resulting cells.

Intrinsic and scale-dependent properties of CNTs has made them a primary choice for studying NF array behavior, and previous work on aligned CNTs has shown that their morphology can be tuned to form complex three-dimensional shapes and patterns *via* capillary-mediated densification.[20–22] By utilizing densification approaches, previous studies have shown that CNT architectures with excellent electrical, thermal, and mechanical properties that approach those predicted by early theoretical models can be synthesized, with the potential for mass production.[23–26] Although targeted densification can be achieved *via* various creative approaches, *e.g.* plasma exposure[27] and low pressure sealing,[28] elasto-capillary self-assembly is the most widely utilized technique due to its simplicity and compatibility with scalable manufacturing approaches.[20–22] See Fig. 1 for an overview of capillary densification in aligned CNTs. While the CNT length governs the force balance during elasto-capillary self-assembly,[29–31] where longer CNTs self-organize into larger cells (see Fig. 1b), accurately predicting the geometry of the CNT cellular patterns given a starting NF array morphology (*e.g.* CNT length) is not currently possible. This originates from the large variability in previously reported CNT cell sizes (see Fig. 1c) and (as will be shown herein) non-representative assumptions of the CNT array elastic response,[32–39] which led to a linear scaling law in ref. 32 that leaves several previous observations unexplained. In this report, we use extensive quantification of the CNT cellular network to model the mechanical behavior of CNTs during

[a] *Department of Materials Science and Engineering, Massachusetts Institute of Technology, Cambridge, MA 02139, USA*
[b] *Department of Aeronautics and Astronautics, Massachusetts Institute of Technology, Cambridge, MA 02139, USA. E-mail: iys@alum.mit.edu, wardle@mit.edu*
[c] *Department of Mechanical Engineering, Massachusetts Institute of Technology, Cambridge, MA 02139, USA*

† Electronic supplementary information (ESI) available: Additional data analysis details (Fig. S1); model derivation (eqn (S1)–(S9), Fig. S2, S3, and Table S1); and full data-sets (Tables S2 and S3). See DOI: 10.1039/c7cp06869g

‡ These authors have contributed equally to this work.

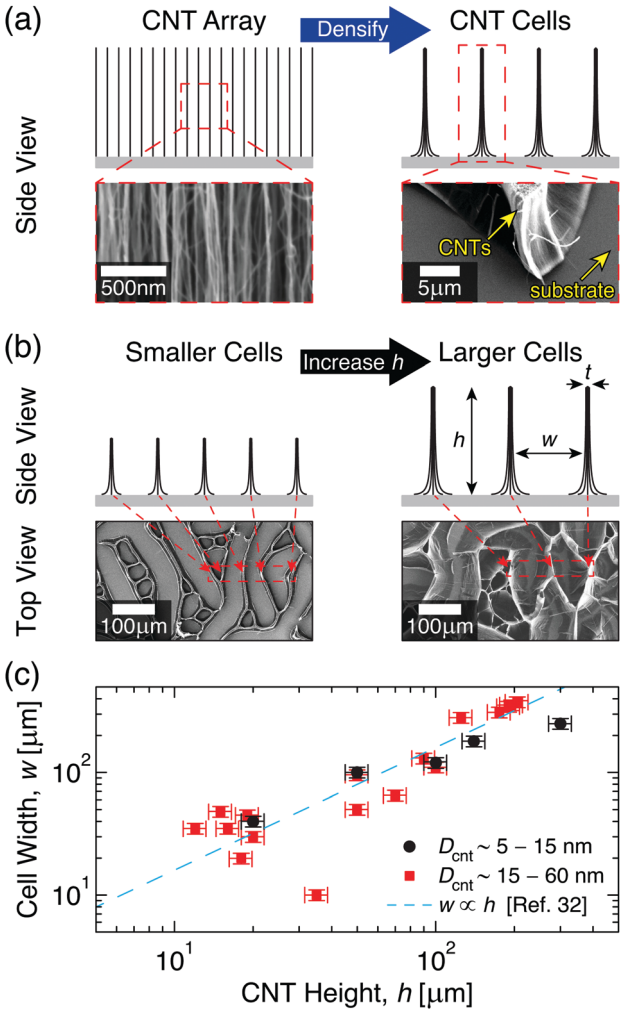

Fig. 1 Capillary-mediated densification of aligned carbon nanotube (CNT) arrays into 2D cellular networks. (a) Illustrations and scanning electron microscopy (SEM) images demonstrating the formation of cells from CNT arrays. (b) Side view illustrations and top view SEM images of CNT cell networks showing that the height (h) of CNT arrays governs the width (w) and wall thickness (t) of the resulting CNT cell, all other factors being the same. (c) Previously reported w of CNT cells made from CNTs with diameters D_{cnt} ~ 5–15 nm to 15–60 nm (●, and ■, respectively),[32–39] and the linear scaling relation proposed in ref. 32.

elasto-capillary self-assembly, and to develop representative scaling relations that accurately predict the evolution of the CNT cell geometry with the height of the initial CNT array.

Aligned CNT arrays were grown in a 22 mm internal diameter quartz tube furnace at atmospheric pressure *via* a previously described thermal catalytic chemical vapor deposition process with ethylene as the carbon source and 600 ppm of water vapor added to the inert gas.[40–42] The CNTs were grown on 1 cm × 1 cm Si substrates *via* a base-growth mechanism on a catalytic layer composed of 1 nm Fe on 10 nm Al_2O_3 deposited *via* electron beam physical vapor deposition.[43–45] The CNTs self-assemble into aligned arrays that were ~10–300 μm tall, and were composed of multiwalled CNTs with an average outer diameter of ~8 nm (3–7 walls with ~5 nm inner diameter and intrinsic CNT density of ≈1.6 g cm^{-3}),[42,45–47] inter-CNT spacing of ~60–80 nm,[48–50] and V_f of ~1% CNTs.[42] To test the impact of CNT adhesion to the growth substrate, a subset of aligned CNTs was heat treated for 40 min at 740 °C under 200 sccm of helium flow, which leads to samples that we call cemented CNTs (→c-CNTs) which are compared to baseline samples that we call not cemented CNTs (→nc-CNTs), *i.e.* nc-CNTs do not undergo thermal post-processing. The cementation post-processing conditions used here originate from a recent study that investigated the tensile force required to remove CNTs from the growth substrate after post-processing for a variety of times and environments at 740 °C (the CNT growth temperature). A maximum of ~4× increase in the CNT-growth substrate adhesion force is reported when compared to the untreated CNTs (*i.e.* nc-CNTs) for samples heat treated in an He ambient for 40 min (additional analysis of these findings is the subject of an upcoming publication).[51] The cementation processing utilized here is similar to other post-growth CNT–substrate adhesion tuning techniques that were investigated in previous studies,[22,52,53] which found that allowing the CNTs to cool in a hydrocarbon ambient increased their adhesion to the growth substrate, and that the CNT–substrate bonding could be weakened *via* etching of the CNT–catalyst interface, *e.g.* using H_2O vapor.[52] The current approach is distinct in its effect and purpose of further increasing the CNT–substrate adhesion. After growth (and cementation processing for c-CNTs), all CNT array samples were then exposed to a previously developed O_2 plasma treatment,[31] and then densified *via* a previously reported paper-soaking technique,[54] which leads to slower wetting and thereby less CNT delamination and damage than direct immersion techniques,[21] using two different solvents (acetone and ethanol). After capillary densification, the cell wall thickness (t) was measured *via* scanning electron microscopy (Zeiss Merlin, 5 mm working distance, 5 kV accelerating voltage). Cell area (A) and circularity (O) were estimated from optical microscope (Carl Zeiss Axiotech 30 HD) images *via* ImageJ (see Section S1 in the ESI† for details),[55] and the cell width (w) was evaluated as a one-dimensional approximation *via* $w \sim \sqrt{A}$. See Fig. 2 for exemplary histograms of t, w, and A. To determine the arithmetic means (Λ), the raw t datasets were analyzed *via* Gaussian distributions, while the raw w and A datasets were analyzed *via* log-normal distributions. Log-normal distributions were used for the raw w and A data because they originate from the time evolution of a Gaussian distribution, *i.e.* the inter-CNT spacing,[16,49,50] without producing new elements, which was postulated to give rise to log-normal statistics in the long-time limit.[56–58] The h dependence of t, w, and A was then investigated by averaging Λ from 2–4 samples, and this is presented in Fig. 3 and Tables S2, S3 in Section S3 of the ESI.†

As Fig. 2a illustrates, the post-processing cementation that creates c-CNTs significantly impacts the self-organization of CNTs into a network of two-dimensional cells. This difference between the cells formed by c-CNTs and those formed by nc-CNTs can be explained by examining the impact of CNT–substrate adhesion on CNT elastic behavior. Although cementation increases CNT–substrate adhesion *via* several mechanisms, this diminished CNT mobility reduces the amount of CNT–CNT junctions that can

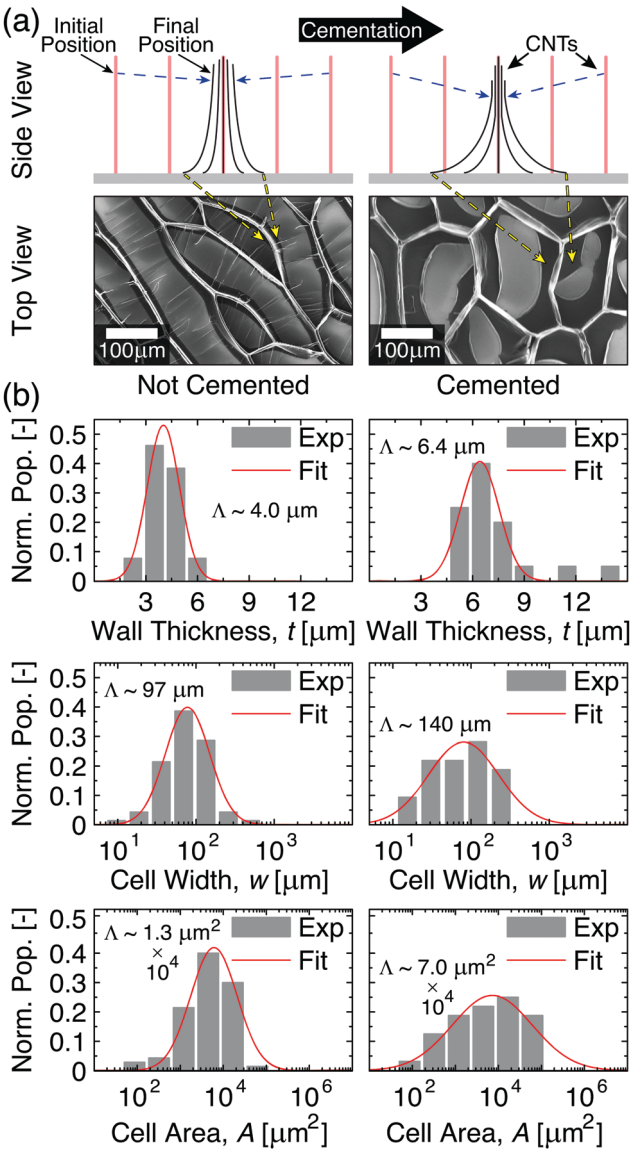

Fig. 2 Effect of CNT–substrate adhesion, either baseline not cemented or cemented *via* post-processing, on CNT cell network formation. (a) Side view illustrations and top view SEM images of cell networks formed from ~35 μm tall CNT arrays. (b) Exemplary distributions of the cell wall thicknesses, cell widths, and areas for CNT cell networks formed using non-cemented (left) and cemented (right) CNT arrays (height ~ 35 μm). Evaluated arithmetic mean (Λ) values indicate that cemented CNTs form larger cells with thicker walls than non-cemented CNTs.

form in the CNT axial direction as the array self-assembles into CNT walls, *i.e.* when the CNTs are deflected perpendicular to their axial direction to form the CNT bundles that comprise the cell walls. Since the torsion deformation mechanism was previously found to contribute >90% of the effective compliance of CNT architectures comprised of weakly interacting CNTs such as those herein,[16] formation of additional CNT–CNT junctions is a mechanism by which the CNTs could collectively reinforce one another and thereby resist deforming *via* torsion. However, because cementation lowers the mobility of CNTs local to the substrate during the capillary-mediated self-assembly process, their ability to entangle with one another in three-dimensional space is likely hindered, which means that the number of CNT–CNT junctions that could be formed along the CNT length in c-CNTs is lower than that of nc-CNTs for a given two-dimensional packing fraction. This effect could be exacerbated by the larger gradient in two-dimensional packing fraction along the length of c-CNTs (see Fig. 2a for illustration) due to lower CNT base mobility when compared to nc-CNTs that can more freely slide and pack. Such a difference in the collective reinforcement efficacy of CNTs with higher substrate adhesion forces implies that the cementation processing would lead c-CNT walls to be less stiff than nc-CNT walls at a comparable t, since c-CNTs would need to achieve a higher three-dimensional volume fraction to reach a similar number of CNT–CNT junctions. Since the capillary forces will be unchanged, this reduction in the wall stiffness as a result of cementation means that, to maintain the force balance, c-CNTs will need to form larger effective bundles. When this is coupled with the diminished CNT mobility perpendicular to their axial direction (due to cementation mediated enhanced substrate adhesion forces), c-CNTs are therefore expected to form larger CNT cells with thicker walls than the cells formed by nc-CNTs. Experimental results support this prediction, as illustrated in histograms of the cell area (A), width (w), and wall thickness (t) for nc- and c-CNTs with $h \sim 35$ μm in Fig. 2b. As seen in Fig. 2b, the evaluated Λ for c-CNTs is significantly larger than for nc-CNTs for t (~6.4 μm *vs.* ~4.0 μm), w (~140 μm *vs.* ~97 μm), and A (~7.0×10^4 μm^2 *vs.* ~1.3×10^4 μm^2), consistent with enhanced substrate adhesion diminishing the CNT cell wall's mechanical reinforcement efficacy. To better understand how cementation affects the mechanics that underpin the formation of CNT cellular networks, models that tie CNT cell geometry to h are discussed next.

To model the capillary-mediated self-organization process of CNT arrays, we assume a one-dimensional point of view for simplicity (as illustrated in Fig. 2a). In this framework, the t for the cell walls can be estimated by starting with the previously derived maximum capillary formed bundle size,[20,59,60] in addition to the recently characterized CNT array morphology,[47–49] which yields the following form:

$$t \approx \Gamma_f \left(\left(\frac{\gamma}{E} \right)^{2/3} \left(\frac{4h^{8/3}}{D_{cnt}{}^2 \Gamma_i^{4/3}} \right) \right)^{1/3} \quad (1)$$

where γ is the surface tension of the solvent (~22 and 25 $\times 10^{-3}$ N m^{-1} for ethanol and acetone used herein, respectively), E is the effective (axial) elastic modulus of the cell wall, which corresponds to the collective elastic response of the tortuous CNTs in the cell wall and is oftentimes orders of magnitude lower than the intrinsic (axial) CNT modulus,[16] Γ_i and Γ_f are the initial (*i.e.* as-grown) and final inter-CNT spacing, D_{cnt} is the CNT outer diameter, and h which is easily quantifiable as the CNT array height and scales with the CNT length. Reasonably good wetting of the CNTs by the solvent is also inherently assumed in eqn (1)[61] (see Section S2 in the ESI† for further details). Assuming that the CNT cells occupy approximately the same total area as the original CNT array, and defining an

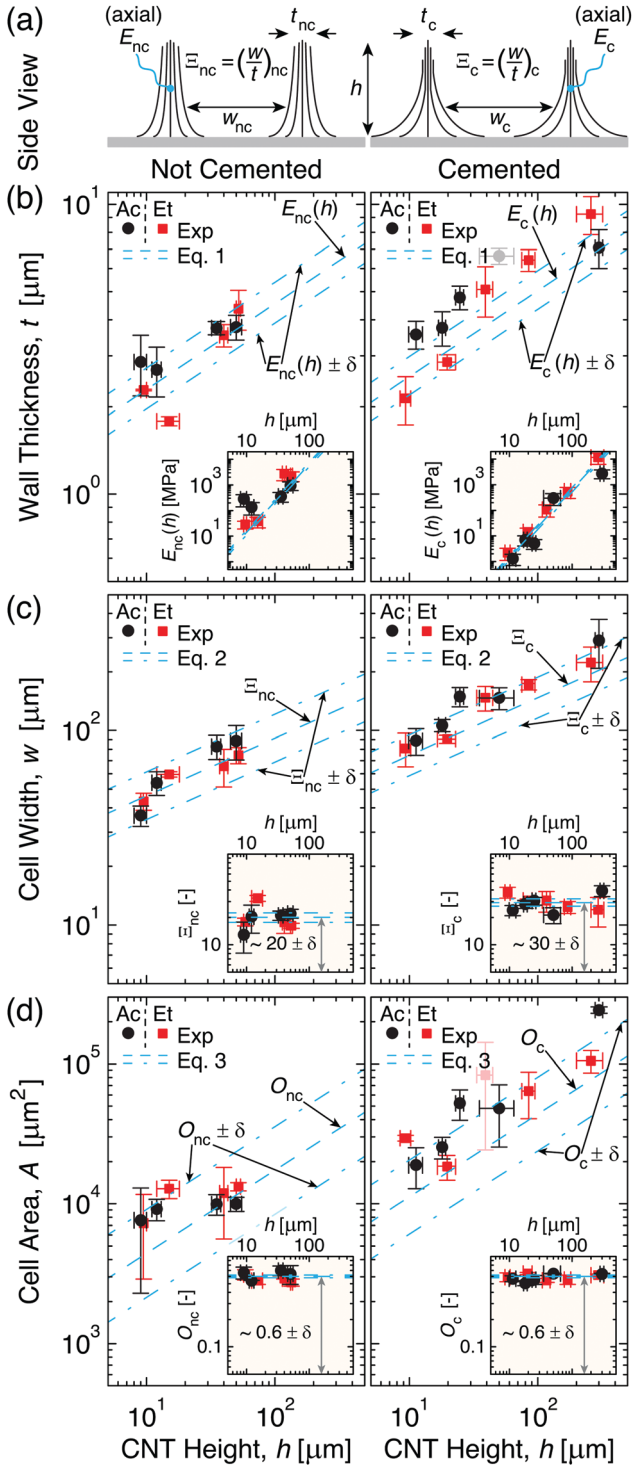

Fig. 3 Cell geometry evolution with CNT height (h) for non-cemented (nc, left) and cemented (c, right) CNTs densified *via* acetone and ethanol (→Ac and Et). (a) Illustrations of different effective wall elastic moduli (E) and densification factors (Ξ) giving rise to thicknesses and widths (t and w) of cells formed from nc- and c-CNTs (→E_{nc}, Ξ_{nc}, t_{nc}, w_{nc} and E_c, Ξ_c, t_c, w_c, respectively). (b) Plot showing that $\partial E_c/\partial h < \partial E_{nc}/\partial h$ leads to faster t scaling with h (eqn (1), see inset) for c-CNTs. (c) Plot illustrating that w scales faster with h (eqn (2), see inset) for c-CNTs because $\Xi_c > \Xi_{nc}$. (d) Plot demonstrating that while cell area (A) scales faster with h (eqn (3), see inset) for c-CNTs, cell circularity (→O_{nc} and O_c) is constant.

average one-dimensional repeat unit of size $w + t$, w can be estimated from t as follows:

$$w \approx t\Xi \quad (2)$$

where Ξ is the densification factor, which is one-dimensional in nature here, as discussed further in Section S2 in the ESI.† Since the one-dimensional framework inherently assumes that the cells are square in shape, while the SEM images in Fig. 1 and 2 illustrate that ellipses are better approximations, A can be approximated from w as follows:

$$A \approx O(\zeta w)^2 \quad (3)$$

where O is a factor accounting for the circularity, and ζ is a correction factor that accounts for the aspect ratio of the ellipses ($\zeta = 1$ for $O = 1 \equiv$ perfectly circular cells) and is discussed further in Section S2 in the ESI.† Using eqn (1)–(3), the experimentally quantified t, w, and A in Fig. 2 can be analyzed from the underlying physics, as presented in Fig. 3.

As Fig. 3 illustrates, t (Fig. 3b), w (Fig. 3c), and A (Fig. 3d) monotonically increase with h for both nc- and c-CNTs (see Fig. 3a for schematic illustrating the two different cell wall geometries, and Section S3 in the ESI† for the raw data). Since acetone and ethanol have very similar values of γ, but very different partial pressures at ambient conditions, Fig. 3 shows that the solvent evaporation rate does not significantly alter the patterns formed since CNTs densified by both acetone and ethanol yield very similar cellular networks. To better understand the effect of cementation on the t scaling with h, E was estimated (*via* eqn (1)) for cell walls comprised of nc- and c-CNTs (see Fig. 3b inset). As Fig. 3b inset illustrates, E scaling with h can be estimated as $E \propto \alpha(h)^{\omega}$ where $\alpha_{nc} \approx 0.030 \pm 0.006 \propto 10 \times \alpha_c$ and $\omega_{nc} = \omega_c \approx 8/3$. This leads to $\partial E_{nc}/\partial h > \partial E_c/\partial h$, which corresponds to $t_{nc} < t_c$ at constant h (*e.g.* Fig. 2b), and is consistent with the previous discussion of lower CNT mobility reducing the effective cell wall stiffness. Additionally, because c-CNTs are harder to delaminate, Fig. 3b indicates that cellular pattern formation is possible at $h > 300$ μm for c-CNTs, which is significantly larger than the maximum $h \sim 60$ μm at which nc-CNTs delaminate from the substrate (and subsequently collapse) due to capillary forces. To elucidate how altering the CNT substrate adhesion influences CNT densification in the cell walls, Ξ was approximated using eqn (2) for CNT cells formed from nc- and c-CNTs (see Fig. 3c inset). As Fig. 3c inset illustrates, $\Xi_{nc} < \Xi_c$ (*i.e.* 20 ± 2 *vs.* 30 ± 3), which leads to $w_{nc} < w_c$ at comparable values of h. Ξ_c leads to a CNT volume fraction in the cell walls of ~30–40%, which is very similar to the maximum packing fraction estimated for similar CNTs (~40 vol% CNTs).[62] This indicates that the densification of c-CNTs is well described by a one-dimensional mechanism similar to how the scaling of the effective indentation modulus of CNT arrays was modeled.[62] However, because Ξ_{nc} is significantly lower than Ξ_c, densification in nc-CNTs may not be purely one-dimensional in nature, since nc-CNTs are able to more freely translate and re-orient themselves with respect to their neighbors, requiring further consideration of two-dimensional interactions.

To further investigate two-dimensional densification effects, O for nc- and c-CNTs was approximated using eqn (3) (see Fig. 3d inset). As the inset of Fig. 3d demonstrates, O is surprisingly found to be of similar magnitude for both nc- and c-CNTs (*i.e.* $O_{nc} \approx 0.60 \pm 0.04$ and $O_c \approx 0.58 \pm 0.02$), which indicates crack initiation and propagation in the CNT arrays, and leads to formation of anisotropic cells with aspect ratios $\sim 3.5 \pm 0.3$ (see Section S2 in the ESI† for details), that is likely dependent on spatial variations in number density and tortuosity of the CNTs that originate from the CNT growth process.[63–66] These results indicate that although the one-dimensional simplifications used here can capture the underlying physical mechanisms that govern cell formation, and thereby yield predictions that agree well with the experimental data presented in Fig. 3, further work that quantifies and simulates topological inhomogeneities present within the CNT arrays is needed to better model CNT cellular network formation in two-dimensions. Note that experimental quantification of such features in as-grown NF arrays is quite challenging.

In summary, the impact of carbon nanotube (CNT) length on capillary-mediated self-assembly of aligned CNT arrays into two-dimensional cellular networks was quantified under conditions that varied the densification solvent and CNT array height, and scaling relations that accurately predict geometry of the resulting CNT cells are presented. The experimental results indicate that CNT cell width, area, and wall thickness increase monotonically as a function of the CNT array height (h). Additionally, by modifying the CNT substrate adhesion force through a post-processing step termed cementation, we find that CNT cells can be made at larger h, since CNT junction interactions are diminished, and that cells formed from cemented CNTs (c-CNTs) counterintuitively exhibit larger width, area, and wall thicknesses compared to their non-cemented CNT (nc-CNT) counterparts at constant h. Modeling illustrates that this originates from how the effective axial elastic modulus (E) of CNTs increases with packing density, and that by reducing CNT mobility, cementation reduces the effective array stiffness of the c-CNTs *vs.* the baseline nc-CNT arrays. Also, modeling indicates that the densification of c-CNTs is approximately one-dimensional in nature, while nc-CNT densification might experience two-dimensional effects. Investigation of CNT cell aspect ratio and circularity shows no statistically significant difference between c-CNTs and nc-CNTs, illustrating that further work building on recent advances in two-dimensional meso-scale simulation of self-organization of such nano-systems due to capillary forces is needed.[67–69] Additionally, since cementation modifies the cellular pattern formation by altering the CNT substrate adhesion force (F_a), but data that could allow the characterization and modeling of the physics and/or chemical mechanisms that gives rise to the observed enhancement in F_a (*e.g.* CNT–CNT, CNT–catalyst, catalyst–substrate or combination thereof) is not currently available, additional work is required to quantify and predict how F_a scales with processing conditions. Once F_a and two-dimensional densification effects can be precisely described and modeled, capillary-mediated densification could be used to inexpensively, quickly, and accurately design bulk nanofiber systems with tuned topologies that could enable next-generation processors, batteries, and lightweight structures.

Conflicts of interest

There are no conflicts of interest to declare.

Acknowledgements

This work was partially supported by Airbus, ANSYS, Embraer, Lockheed Martin, Saab AB, Saertex, and TohoTenax through MIT's Nano-Engineered Composite Aerospace STructures (NECST) Consortium, and partially supported by the National Aeronautics and Space Administration (NASA) Space Technology Research Institute (STRI) for Ultra-Strong Composites by Computational Design (US-COMP), grant number NNX17AJ32G. The authors thank Dr S. Kim (MIT) and Prof. A. J. Hart (MIT) for help with O_2 plasma treatment, D. Lidston (MIT) for help with cementation processing, and the members of necstlab at MIT for technical support and advice. This work made use of the MIT Materials Research Laboratory (MRL) Shared Experimental Facilities, supported in part by the MRSEC Program of the National Science Foundation under award number DMR-1419807, and was carried out in part through the use of MIT's Microsystems Technology Laboratories.

References

1 D. Xiang, X. Wang, C. Jia, T. Lee and X. Guo, *Chem. Rev.*, 2016, **116**, 4318–4440.
2 M. M. Shulaker, G. Hills, N. Patil, H. Wei, H.-Y. Chen, H.-S. P. Wong and S. Mitra, *Nature*, 2013, **501**, 526–530.
3 M. M. Shulaker, G. Hills, R. S. Park, R. T. Howe, K. Saraswat, H.-S. P. Wong and S. Mitra, *Nature*, 2017, **547**, 74–78.
4 W. Wu, *Nanoscale*, 2017, **9**, 7342–7372.
5 H. Sun, Y. Zhang, J. Zhang, X. Sun and H. Peng, *Nat. Rev. Mater.*, 2017, **2**, 17023.
6 J. Ni and Y. Li, *Adv. Energy Mater.*, 2016, **6**, 1600278.
7 L. Mai, X. Tian, X. Xu, L. Chang and L. Xu, *Chem. Rev.*, 2014, **114**, 11828–11862.
8 K. Cui, T. Chiba, S. Omiya, T. Thurakitseree, P. Zhao, S. Fujii, H. Kataura, E. Einarsson, S. Chiashi and S. Maruyama, *J. Phys. Chem. Lett.*, 2013, **4**, 2571–2576.
9 J. Zhang, X. Liu, G. Neri and N. Pinna, *Adv. Mater.*, 2016, **28**, 795–831.
10 J. F. Fennell, S. F. Liu, J. M. Azzarelli, J. G. Weis, S. Rochat, K. A. Mirica, J. B. Ravnsbæk and T. M. Swager, *Angew. Chem., Int. Ed.*, 2016, **55**, 1266–1281.
11 G. V. Stoychev and L. Ionov, *ACS Appl. Mater. Interfaces*, 2016, **8**, 24281–24294.
12 L. Kong and W. Chen, *Adv. Mater.*, 2014, **26**, 1025–1043.
13 S. K. Kumar, B. C. Benicewicz, R. A. Vaia and K. I. Winey, *Macromolecules*, 2017, **50**, 714–731.
14 A. K. Naskar, J. K. Keum and R. G. Boeman, *Nat. Nanotechnol.*, 2016, **11**, 1026–1030.

15 M. F. L. De Volder, S. H. Tawfick, R. H. Baughman and A. J. Hart, *Science*, 2013, **339**, 535–539.
16 I. Y. Stein, D. J. Lewis and B. L. Wardle, *Nanoscale*, 2015, **7**, 19426–19431.
17 B. Natarajan, N. Lachman, T. Lam, D. Jacobs, C. Long, M. Zhao, B. L. Wardle, R. Sharma and J. A. Liddle, *ACS Nano*, 2015, **9**, 6050–6058.
18 I. Y. Stein and B. L. Wardle, *Nanotechnology*, 2016, **27**, 035701.
19 Z. Hu, C. Uzun, Z. Dong, W. Li, A. A. Bernussi and G. Kumar, *Appl. Phys. Lett.*, 2017, **111**, 023107.
20 S. H. Tawfick, J. Bico and S. Barcelo, *MRS Bull.*, 2016, **41**, 108–114.
21 M. De Volder and A. J. Hart, *Angew. Chem., Int. Ed.*, 2013, **52**, 2412–2425.
22 M. De Volder, S. H. Tawfick, S. J. Park, D. Copic, Z. Zhao, W. Lu and A. J. Hart, *Adv. Mater.*, 2010, **22**, 4384–4389.
23 L. Zhang, G. Zhang, C. Liu and S. Fan, *Nano Lett.*, 2012, **12**, 4848–4852.
24 J. Di, X. Wang, Y. Xing, Y. Zhang, X. Zhang, W. Lu, Q. Li and Y. T. Zhu, *Small*, 2014, **10**, 4606–4625.
25 Q. Liu, M. Li, Y. Gu, Y. Zhang, S. Wang, Q. Li and Z. Zhang, *Nanoscale*, 2014, **6**, 4338–4344.
26 Y. Wang, M. Li, Y. Gu, X. Zhang, S. Wang, Q. Li and Z. Zhang, *Nanoscale*, 2015, **7**, 3060–3066.
27 W. Wang, I. Ruiz, K. Ahmed, H. H. Bay, A. S. George, J. Wang, J. Butler, M. Ozkan and C. S. Ozkan, *Small*, 2014, **10**, 3389–3396.
28 T. Wang, K. Jeppson and J. Liu, *Carbon*, 2010, **48**, 3795–3801.
29 S. Tawfick, Z. Zhao, M. Maschmann, A. Brieland-Shoultz, M. De Volder, J. W. Baur, W. Lu and A. J. Hart, *Langmuir*, 2013, **29**, 5190–5198.
30 S. Tawfick, M. De Volder and A. J. Hart, *Langmuir*, 2011, **27**, 6389–6394.
31 M. F. L. D. Volder, S. J. Park, S. H. Tawfick, D. O. Vidaud and A. J. Hart, *J. Micromech. Microeng.*, 2011, **21**, 045033.
32 N. Chakrapani, B. Wei, A. Carrillo, P. M. Ajayan and R. S. Kane, *Proc. Natl. Acad. Sci. U. S. A.*, 2004, **101**, 4009–4012.
33 S. Kaur, S. Sahoo, P. Ajayan and R. Kane, *Adv. Mater.*, 2007, **19**, 2984–2987.
34 H. Liu, S. Li, J. Zhai, H. Li, Q. Zheng, L. Jiang and D. Zhu, *Angew. Chem., Int. Ed.*, 2004, **43**, 1146–1149.
35 Q. Li, R. DePaula, X. Zhang, L. Zheng, P. N. Arendt, F. M. Mueller, Y. T. Zhu and Y. Tu, *Nanotechnology*, 2006, **17**, 4533.
36 M. A. Correa-Duarte, N. Wagner, J. Rojas-Chapana, C. Morsczeck, M. Thie and M. Giersig, *Nano Lett.*, 2004, **4**, 2233–2236.
37 K. Zhang, T. Li, L. Ling, H. Lu, L. Tang, C. Li, L. Wang and Y. Yao, *Carbon*, 2017, **114**, 435–440.
38 A. Qiu and D. F. Bahr, *Carbon*, 2013, **55**, 335–342.
39 L. F. Dumée, K. Sears, J. A. Schütz, N. Finn, M. Duke, S. Mudie, N. Kirby and S. Gray, *J. Colloid Interface Sci.*, 2013, **407**, 556–560.
40 J. Lee, I. Y. Stein, S. S. Kessler and B. L. Wardle, *ACS Appl. Mater. Interfaces*, 2015, **7**, 8900–8905.
41 I. Y. Stein, A. L. Kaiser, A. J. Constable, L. Acauan and B. L. Wardle, *J. Mater. Sci.*, 2017, **52**, 13799–13811.
42 J. Lee, I. Y. Stein, M. E. Devoe, D. J. Lewis, N. Lachman, S. S. Kessler, S. T. Buschhorn and B. L. Wardle, *Appl. Phys. Lett.*, 2015, **106**, 053110.
43 A. J. Hart and A. H. Slocum, *J. Phys. Chem. B*, 2006, **110**, 8250–8257.
44 D. Handlin, I. Y. Stein, R. Guzman de Villoria, H. Cebeci, E. M. Parsons, S. Socrate, S. Scotti and B. L. Wardle, *J. Appl. Phys.*, 2013, **114**, 224310.
45 I. Y. Stein and B. L. Wardle, *Carbon*, 2014, **68**, 807–813.
46 N. Lachman, I. Y. Stein, A. Ugur, D. L. Lidston, K. K. Gleason and B. L. Wardle, *Nanotechnology*, 2017, **28**, 24LT01.
47 I. Y. Stein, N. Lachman, M. E. Devoe and B. L. Wardle, *ACS Nano*, 2014, **8**, 4591–4599.
48 I. Y. Stein and B. L. Wardle, *Phys. Chem. Chem. Phys.*, 2013, **15**, 4033–4040.
49 I. Y. Stein and B. L. Wardle, *Phys. Chem. Chem. Phys.*, 2016, **18**, 694–699.
50 H. K. Mutha, Y. Lu, I. Y. Stein, H. J. Cho, M. E. Suss, T. Laoui, C. V. Thompson, B. L. Wardle and E. N. Wang, *Nanotechnology*, 2017, **28**, 05LT01.
51 D. L. Lidston, MSc thesis, Massachusetts Institute of Technology, 2017.
52 C. L. Pint, Y.-Q. Xu, M. Pasquali and R. H. Hauge, *ACS Nano*, 2008, **2**, 1871–1878.
53 M. Bedewy, *J. Mater. Res.*, 2017, **32**, 153–165.
54 D. Jiang, T. Wang, S. Chen, L. Ye and J. Liu, *Microelectron. Eng.*, 2013, **103**, 177–180.
55 C. A. Amadei, I. Y. Stein, G. J. Silverberg, B. L. Wardle and C. D. Vecitis, *Nanoscale*, 2016, **8**, 6783–6791.
56 M. Y. Choi, H. Choi, J.-Y. Fortin and J. Choi, *Europhys. Lett.*, 2009, **85**, 30006.
57 S. Goh, H. W. Kwon, M. Y. Choi and J.-Y. Fortin, *Phys. Rev. E: Stat., Nonlinear, Soft Matter Phys.*, 2010, **82**, 061115.
58 S. Goh, H. W. Kwon and M. Y. Choi, *J. Phys. A: Math. Theor.*, 2014, **47**, 225101.
59 F. Chiodi, B. Roman and J. Bico, *Europhys. Lett.*, 2010, **90**, 44006.
60 C. Py, R. Bastien, J. Bico, B. Roman and A. Boudaoud, *Europhys. Lett.*, 2007, **77**, 44005.
61 J. Qiu, J. Terrones, J. J. Vilatela, M. E. Vickers, J. A. Elliott and A. H. Windle, *ACS Nano*, 2013, **7**, 8412–8422.
62 H. Cebeci, I. Y. Stein and B. L. Wardle, *Appl. Phys. Lett.*, 2014, **104**, 023117.
63 M. R. Maschmann, *Carbon*, 2015, **86**, 26–37.
64 V. Balakrishnan, M. Bedewy, E. R. Meshot, S. W. Pattinson, E. S. Polsen, F. Laye, D. N. Zakharov, E. A. Stach and A. J. Hart, *ACS Nano*, 2016, **10**, 11496–11504.
65 E. R. Meshot, D. W. Zwissler, N. Bui, T. R. Kuykendall, C. Wang, A. Hexemer, K. J. J. Wu and F. Fornasiero, *ACS Nano*, 2017, **11**, 5405–5416.
66 W. Shi, J. Li, E. S. Polsen, C. R. Oliver, Y. Zhao, E. R. Meshot, M. Barclay, D. H. Fairbrother, A. J. Hart and D. L. Plata, *Nanoscale*, 2017, **9**, 5222–5233.
67 H.-W. Pei, H. Liu, Z.-Y. Lu and Y.-L. Zhu, *Phys. Rev. E: Stat., Nonlinear, Soft Matter Phys.*, 2015, **91**, 020401.
68 H.-W. Pei, H. Liu, Y.-L. Zhu and Z.-Y. Lu, *Phys. Chem. Chem. Phys.*, 2016, **18**, 18767–18775.
69 H.-W. Pei, X.-L. Liu, H. Liu, Y.-L. Zhu and Z.-Y. Lu, *Phys. Chem. Chem. Phys.*, 2017, **19**, 4710–4718.